Article

Spontaneous Etching of Metal Fluorides Using Ligand-Exchange Reactions: Landscape Revealed by Mass Spectrometry

Ann Lii-Rosales, Andrew S. Cavanagh, Andreas Fischer, Thorsten Lill, and Steven M. George*

ACCESS | 📊 Metrics & More | 📖 Article Recommendations | 🄢ᴵ Supporting Information

ABSTRACT: Thermal atomic layer etching (ALE) can be performed using sequential reactions based on surface modification followed by volatile release of the modified surface layer. Surface modification can be accomplished using fluorination. Volatile release can then be achieved using precursors that undergo ligand-exchange reactions with the fluorinated surface layer. Metal fluorides can be employed to model the fluorinated surface layer. The ligand-exchange reaction between the precursor and the metal fluoride can lead to spontaneous etching of the metal fluoride. A new reactor with *in situ* quadrupole mass spectrometry (QMS) was constructed to observe the volatile etch products from the reaction of ligand-exchange precursors with metal fluoride powders. The metal fluoride powders were AlF_3, HfF_4, GaF_3, InF_3, and SnF_4. The ligand-exchange precursors were $Al(CH_3)_3$, $SiCl_4$, and $TiCl_4$. A variety of studies were conducted including $Al(CH_3)_3$ + AlF_3, $SiCl_4$ + HfF_4, $SiCl_4$ + InF_3, $TiCl_4$ + SnF_4, $Al(CH_3)_3$ + GaF_3, and $SiCl_4$ + AlF_3. The temperature-dependent *in situ* QMS studies revealed the many possibilities that occur during the ligand-exchange reaction of precursors with metal fluoride powders. Various categories of behavior were observed from these studies: (i) Ligand exchange occurs at low temperature, but metal etch products from the substrate are not observed until high temperature. (ii) Ligand-exchange and metal etch products from the substrate are observed at similar temperatures. (iii) Ligand exchange occurs, but no metal etch products from the substrate are observed up to a limiting temperature. Knowledge of these possibilities for the ligand-exchange reaction between precursors and metal fluoride powders during spontaneous etching helps to further the understanding of thermal ALE.
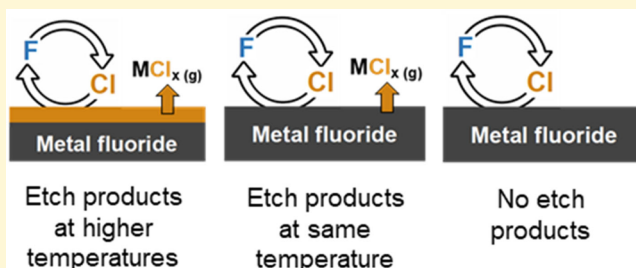
I. INTRODUCTION

Thermal atomic layer etching (ALE) utilizes sequential, self-limiting surface reactions to remove material with atomic level precision.[1,2] Thermal ALE consists of two reactions: (A) surface modification and (B) removal of the modified surface layer via volatilization.[1] Many materials can be etched using thermal ALE.[3] These materials include metal oxides such as Al_2O_3,[2,4,5] HfO_2,[6,7] ZnO,[8] Ga_2O_3,[9] and WO_3,[10] metal nitrides such as AlN,[11] TiN,[12] and GaN,[13] semiconductor materials such as Si,[14] SiO_2,[15] and Si_3N_4,[16] and metals such as W,[10] Cu,[17] and Co.[18] Thermal ALE will be critical to provide atomic layer precision for etching to fabricate advanced three-dimensional semiconductor devices.[19]

For metal oxide thermal ALE, surface modification often involves fluorination typically using HF.[1,2,20] This fluorination creates a surface layer of metal fluoride.[21] A strategy for volatilization can then employ ligand-exchange reactions.[1,2,22] The ligand exchange of F for Cl is an effective pathway because metal chlorides are generally more volatile than their corresponding fluorides. The ligand exchange of F for CH_3 is also a viable possibility because metal alkyls typically have much higher vapor pressure than metal fluorides.

Both surface modification and volatile release reactions are necessary for thermal ALE. Using the fluorination and ligand-

exchange mechanism, the material removal occurs only during the ligand-exchange reaction.[1,22] The spontaneous etching of metal fluoride powders using ligand-exchange precursors can serve as a model to understand the ligand-exchange reactions occurring during thermal ALE.[23] In addition, the spontaneous etching of metal fluorides by ligand-exchange reactions is a new gas phase etching mechanism. There are only a few other examples of dry thermal spontaneous etching. The main demonstrations involve etching by the formation of volatile fluorides using fluorination reactants such as XeF_2 or HF vapor.[24−27]

The spontaneous etching of AlF_3 using $Al(CH_3)_3$ was studied earlier using *in situ* QMS to understand thermal Al_2O_3 ALE using HF and TMA as the reactants.[23] Various $Al_xF_y(CH_3)_z^+$ species were identified as the volatile metal etch products produced by the ligand-exchange reactions.[23]
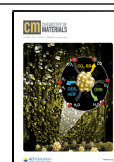
The previous QMS reactor utilized static dosing and the reactor design did not allow for line-of-sight detection of the reaction products.

To obtain higher sensitivity for detection of volatile etch products, a new reactor with *in situ* QMS was constructed and employed for the present work. This new QMS reactor enabled rapid assessment of volatile etch products during spontaneous etching of metal fluoride powders by ligand-exchange precursors. The temperature of metal fluoride powders could also be easily ramped for real-time monitoring of the etch products versus temperature. In addition, the precursors and products were entrained in a molecular beam for line-of-sight detection to increase their signal intensity and minimize their interactions with the walls of the vacuum chamber prior to QMS detection.

Using this new QMS reactor, various ligand-exchange precursors and metal fluoride powders were studied to explore the spontaneous etching of metal fluorides. The metal fluoride powders were AlF_3, HfF_4, GaF_3, InF_3, and SnF_4. The ligand-exchange precursors were $Al(CH_3)_3$, $SiCl_4$ and $TiCl_4$. These metal fluorides and ligand-exchange precursors include combinations that represent reactions that have been employed previously for thermal ALE. These combinations have been both successful and unsuccessful for thermal ALE. In addition, some of these combinations represent reactions that have not yet been investigated for thermal ALE and should provide predictions for thermal ALE.

The studies that were associated with reported thermal ALE systems were $Al(CH_3)_3$ + AlF_3,[4] $SiCl_4$ + HfF_4[28] and $Al(CH_3)_3$ + GaF_3.[9] These investigations model thermal Al_2O_3 ALE using HF and TMA,[4] HfO_2 ALE using HF and $SiCl_4$,[28] and Ga_2O_3 ALE using HF and TMA,[9] respectively. The QMS studies that were not yet related to known thermal ALE systems were $SiCl_4$ + InF_3 and $TiCl_4$ + SnF_4. These investigations should be predictive of thermal ALE of In_2O_3 and SnO_2 using HF and either $SiCl_4$ or $TiCl_4$ as the reactants. In addition, the QMS study that was associated with a thermal ALE process that did not lead to etching was $SiCl_4$ + AlF_3. The lack of etching agrees with earlier investigations that reported that thermal Al_2O_3 ALE did not occur with HF and $SiCl_4$ as the reactants.[28]

The temperature dependence of these various reactions revealed several categories of behavior during ligand exchange. For example, the temperature dependence of some of the combinations of ligand-exchange precursors and metal fluoride powders indicate that ligand exchange can occur at low temperature in advance of the appearance of the metal etch products from the substrate at high temperature. Other combinations show that ligand-exchange and metal etch products from the substrate can be observed at similar temperatures. Additional combinations observe that ligand exchange can occur without producing metal etch products from the substrate up to a limiting high temperature. These studies reveal the spectrum of possibilities for spontaneous etching of metal fluorides using ligand-exchange reactions.

II. EXPERIMENTAL SECTION

II.A. Overview of Reactor. A new reactor was used to perform the *in situ* QMS studies of reactions between ligand-exchange precursors and metal fluoride powders. The reactor assembly shown in Figure 1 consisted of a precursor manifold with six precursor lines and a precursor reservoir (Figure 1A). A gas inlet connected the reservoir to the sample housing (Figure 1B) where the metal fluoride powders were exposed to the ligand-exchange precursors. An
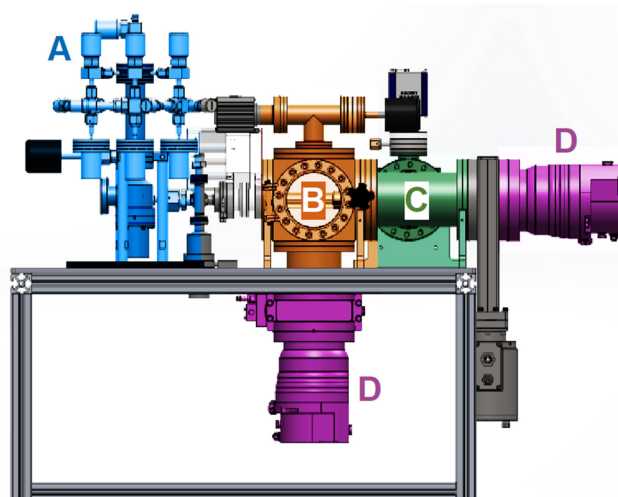

Figure 1. Schematic of the quadrupole mass spectrometry (QMS) reactor: (A) precursor manifold; (B) sample housing and differentially pumped region; (C) differentially pumped QMS chamber; and (D) turbomolecular pumps.

additional gas inlet with N_2 carrier gas at pressures ranging from 1 to 2 Torr was connected to the sample housing to transport the gas-phase species. Further details of the precursor manifold are included in the Supporting Information.

The volatile etch species produced during the ligand-exchange reactions and the N_2 carrier gas could exit the sample housing through an aperture and enter a differentially pumped chamber outside the sample housing. This created a molecular beam that could further transport the volatile etch species through a skimmer and into the QMS chamber (Figure 1, C). The QMS chamber was maintained at low pressure by differential pumping with a turbomolecular pump (Figure 1, D). During reactions, the typical pressure was 2−3 Torr in the sample housing, $1−2 \times 10^{-5}$ Torr in the differentially pumped region outside the sample housing, and low 10^{-7} or high 10^{-8} Torr in the differentially pumped QMS chamber.

II.B. Sample Housing and Heating. The ligand-exchange reactions were performed inside the sample housing shown in Figure 2. A copper block (Figure 2, A) defined the sample housing assembly that was suspended to reduce thermal contact with the vacuum walls to achieve efficient heating. Two heater cartridges (Figure 2, B; Valin Corporation) were inserted into the copper block to enable heating of
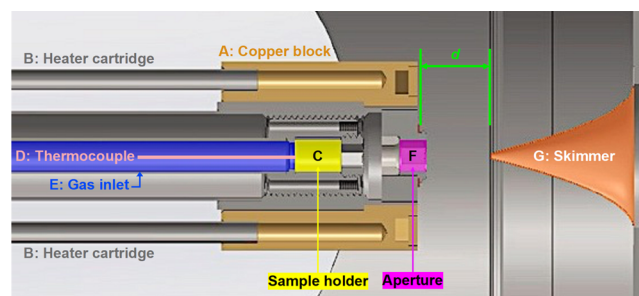

Figure 2. Expansion of the sample housing and surrounding differentially pumped region. (A) Copper block; (B) heater cartridges; (C) sample holder for powder samples; (D) *in situ* thermocouple that contacts back side of sample holder; (E) gas inlet tube for N_2 carrier gas and ligand-exchange precursors; (F) aperture of sample housing; and (G) skimmer that separates the differentially pumped region outside the sample housing from the QMS chamber. Distance (d) is the adjustable distance between the sample housing aperture and the skimmer.

the copper block and the powder sample inside the sample holder (Figure 2, C).

The maximum achievable temperature was ~530 °C. A typical temperature ramp of 3 °C/min was used to heat the sample. The temperature of the sample holder was measured *in situ* during the reactions by a K-type thermocouple (Figure 2, D). The thermocouple was installed through the gas inlet tube (Figure 2, E) and contacted the back mesh of the sample holder.

An aperture (Figure 2, F) with a diameter of 300 μm was located on the face of the sample housing assembly. The volatile etch species could pass through this aperture to enter the differentially pumped region outside the sample housing. Additional description of the sample housing and gas expansion upon exiting the sample housing is contained in the Supporting Information.

II.C. Molecular Beam Generation and Skimmer. The N_2 carrier gas is the major component of the molecular beam. This N_2 carrier gas entrains the volatile etch species produced during the ligand-exchange reaction between the precursors and the metal fluoride powders. Beam generation occurs because of gas expansion resulting from the large pressure differential between a high backing pressure (P_0) in the sample housing behind the aperture and the low pressure (P_1) in the expansion area in the differentially pumped region outside of the sample housing.

A parabolic-shaped skimmer (Figure 2, G) was aligned with line-of-sight to the aperture on the sample housing and the QMS ionizer entrance. The distance, d, between the sample housing aperture and the skimmer is shown in Figure 2. This distance could be adjusted using a linear-motion feedthrough with a 50 mm range connected to the sample housing assembly.

The apertures, gas flow, and operating pressures are depicted in Figure 3. Alignment was achieved by passing a laser beam through all
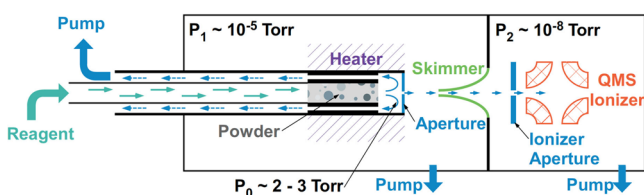

Figure 3. Schematic of gas flows and pressures in the QMS reactor. Aperture, skimmer, and QMS ionizer are all on the same line center.

three apertures (sample housing, skimmer, and QMS ionizer) from one end of the reactor to another. In addition, the alignment and molecular beam behavior were confirmed by monitoring the intensity of the N_2 carrier gas by QMS as a function of d. More details about the molecular beam and skimmer can be found in the Supporting Information.

II.D. Quadrupole Mass Spectrometry. Detection of volatile species was accomplished using a quadrupole mass spectrometer (Extrel, MAX-QMS Flange Mounted System). To minimize exposures to corrosive gaseous species, the ionizer and analyzer were positioned perpendicular to the incoming molecular beam. An electron ionization energy of 70 eV was used in the experiments. Each QMS scan ranging 1−1000 amu was completed in 2.2 s with 27 data points per amu. The scans were recorded throughout the temperature ramp during the experiments. Further details about the QMS signal detection are contained in the Supporting Information.

II.E. Chemicals for the Ligand-Exchange Reactions. Metal fluoride powders used in the experiments included AlF_3 (anhydrous, 99.8%, Sigma-Aldrich), HfF_4 (99.9%, Sigma-Aldrich), InF_3 (≥99.9%, Sigma-Aldrich), SnF_4 (Sigma-Aldrich), and GaF_3 (anhydrous, 99.85%, Alfa Aesar). The mass of the metal fluoride powder was typically ≤0.1 g.

The ligand-exchange precursors included $Al(CH_3)_3$ (97%, Sigma-Aldrich), $SiCl_4$ (99%, Sigma-Aldrich), and $TiCl_4$ (99.9%, Sigma-Aldrich). The partial pressure of the ligand-exchange precursor that flowed through the metal fluoride powders ranged from 0.04 to 0.15

Torr. This pressure was calculated from the difference between the sample housing pressure before and after introducing the ligand-exchange precursor. Additional description about the N_2 carrier gas that transports the precursors and reaction products is contained in the Supporting Information.

III. RESULTS AND DISCUSSION

III.A. $Al(CH_3)_3$ + AlF_3. The initial *in situ* QMS studies examined the volatile etch products produced during the spontaneous etching of AlF_3 powder by TMA.[4,23,29] These studies were performed to benchmark the new reactor by comparison with the previous QMS studies of thermal Al_2O_3 ALE using HF and $Al(CH_3)_3$ (trimethylaluminum, TMA), as well as the spontaneous etch of AlF_3 powder using TMA.[23] The earlier QMS studies of ligand exchange between AlF_3 and TMA were performed at 300 °C. The major etch products identified by the previous QMS studies were dimers of dimethylaluminum fluoride (DMAF) with itself (DMAF/DMAF) and with TMA (DMAF/TMA).[23] These dimers were observed as $Al_2F(CH_3)_4^+$ at m/z = 133 amu and $Al_2F_2(CH_3)_3^+$ at m/z = 137 amu. Each of these dimers presumably lost one CH_3 group during electron impact ionization to form the observed ion. In addition, there was an Al trimer that was observed as $Al_3F_3(CH_3)_5^+$ at m/z = 213 amu.[23]

The *in situ* QMS results for the AlF_3 + TMA system in this study were similar to the earlier results. Figure 4 shows the

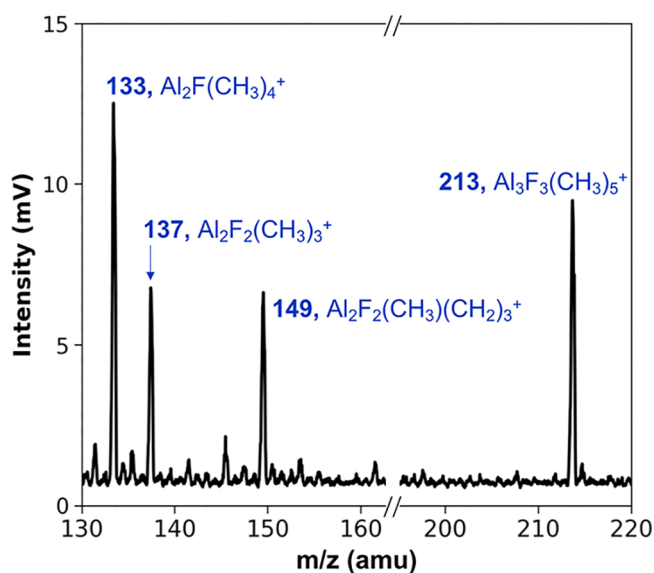**Figure 4.** Mass spectrum showing dominant ion signals of Al etch products at m/z = 133, 137, 149, and 213 amu during reaction between $Al(CH_3)_3$ and AlF_3 powder at 200 °C.

observed mass spectrum at 200 °C that reveals the same Al dimers at m/z = 133 and m/z = 137 amu, as well as the Al trimer at m/z = 213 amu. In addition, a new Al dimer is observed as $Al_2F_2(CH_3)(CH_2)_3^+$ at m/z = 149 amu. By entraining the etch products in a molecular beam and having line-of-sight delivery to the QMS ionizer, the new QMS reactor increased detection sensitivity and minimized wall effects. The observation of this new dimer at 200 °C may be attributed to the new QMS reactor design. Alternatively, the new dimer at m/z = 149 amu may have a much lower intensity at the higher temperature of 300 °C used in the previous study.

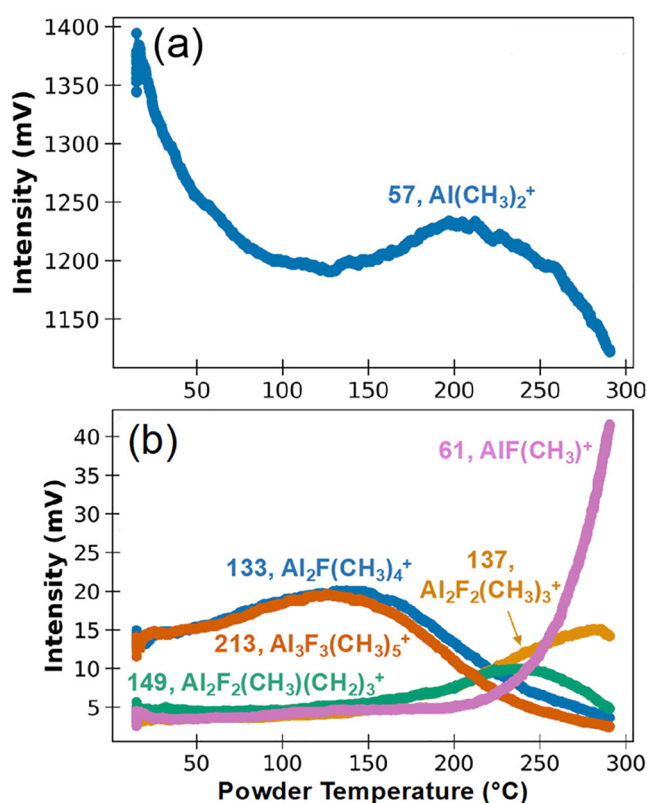The new QMS reactor is also capable of obtaining temperature-dependent results. Figure 5a shows the intensity

Figure 5. Ion signal intensities of (a) $Al(CH_3)_2^+$ and (b) Al etch products versus powder temperature during reaction between $Al(CH_3)_3$ and AlF_3 powder. The most intense isotope peak of each species was employed in the plots.

of $Al(CH_3)_2^+$ at $m/z = 57$ amu as a function of powder temperature. $Al(CH_3)_2^+$ is the most prominent cracking fragment of TMA resulting from electron impact ionization.[30] As the $Al(CH_3)_2^+$ intensity decreases with increasing temperature, the intensity traces of $Al_2F(CH_3)_4^+$ at $m/z = 133$ amu and $Al_3F_3(CH_3)_5^+$ at $m/z = 213$ amu rise as shown in Figure 5b. This correlation is the expected complementary behavior when the consumption of the TMA precursor gives rise to ligand-exchange products. The $Al(CH_3)_2^+$ intensity reaches a minimum around 125 °C. In comparison, the Al dimer at $m/z = 133$ amu and Al trimer at $m/z = 213$ amu reach their maximum intensities at around 125 °C. The close correlation of the intensities for the Al dimer at $m/z = 133$ amu and Al trimer at $m/z = 213$ amu also suggests that the Al dimer could be a fragment of the Al trimer.

Figure 5b reveals that the signals for the Al dimer at $m/z = 133$ and the Al trimer at $m/z = 213$ amu are already present at the start of the heat ramp at 18 °C. This observation suggests that the ligand-exchange reaction between TMA and AlF_3 is very facile and produces volatile Al products at room temperature. Seeing ligand exchange at room temperature suggests that the temperature dependence observed for Al_2O_3 ALE using HF and TMA as the reactants results from the fluorination reaction.[20] The temperature dependence of the HF fluorination may also explain the higher etch rates for Al_2O_3 ALE observed using SF_4 plasma and TMA as the reactants.[31] The SF_4 plasma may fluorinate the Al_2O_3 more

easily and produce thicker fluoride layers on Al_2O_3 than HF exposures.[20]

The results in Figure 5b also show that the DMAF monomer observed as $AlF(CH_3)^+$ at $m/z = 61$ amu is not observed until higher temperatures >225 °C. The DMAF monomer is the primary etch product expected from the ligand-exchange reaction between TMA and AlF_3.[23] The DMAF monomer is the most abundant etch product at >250 °C. The DMAF monomer may be observed only at higher temperatures when there is enough thermal energy to break the DMAF/TMA and DMAF/DMAF dimer bonds.

The intensities of $Al_2F_2(CH_3)_3^+$ at $m/z = 137$ amu and $Al_2F_2(CH_3)(CH_2)_3^+$ at $m/z = 149$ amu also do not rise until higher temperatures >175 °C. The intensity of the DMAF/DMAF dimer at $m/z = 137$ is increasing as the signals at $m/z = 133$ and $m/z = 213$ amu are decreasing. This correlation may result from the temperature dependence of the TMA coverage on the surface. There may be more TMA on the surface and the DMAF/TMA dimer may be favored at low temperature. In contrast, there may be less TMA on the surface and the DMAF/DMAF dimers may be preferred at higher temperature when DMAF dominates the surface coverage.

The previous *in situ* QMS studies of the spontaneous etching of AlF_3 powder using TMA at 300 °C observed prominent signals at $m/z = 133$, 137, and 213 amu.[23] In contrast, Figure 5b reveals that the main signal intensities at 300 °C in the current study are observed at $m/z = 61$, 137, and 149 amu. These differences could arise from the experiment methodology. The previous study was performed using static TMA exposures for 60 s to react with the AlF_3 powder. In contrast, the present study used a constant flow of TMA precursor. These differences between static exposure and constant flow experiments may indicate that residence time plays a significant role in product formation. A longer residence time for the TMA precursor and DMAF product may favor the production of the dimers and trimers in the static exposure experiments at 300 °C. Only the DMAF monomer at $m/z = 61$ and the DMAF/DMAF dimer at $m/z = 137$ amu have significant intensity in the constant flow experiments at 300 °C.

III.B. SiCl₄ + HfF₄. Additional *in situ* QMS studies examined the volatile etch products produced during the spontaneous etching of HfF_4 powder by $SiCl_4$. This system relates to the previous investigation of thermal HfO_2 ALE using HF and $SiCl_4$ as the reactants.[28] In the thermal HfO_2 ALE experiments, HfO_2 was fluorinated using HF and then $SiCl_4$ was used for the ligand-exchange reaction. The observed HfO_2 etch rate was 0.05 Å/cycle at 350 °C.[28] Thermochemical calculations also showed that the ligand-exchange reaction between $SiCl_4$ and HfF_4 was favorable above 200 °C.[28]

The *in situ* QMS studies identified a variety of $HfF_xCl_y^+$ ion species from the volatile etch products based on their characteristic Hf and Cl isotopes during the spontaneous etching of HfF_4 powder by $SiCl_4$. Results for the $HfFCl_2^+$ ion at 523 °C are shown in Figure 6. The $HfFCl_2^+$ ion has its highest intensity peak at $m/z = 269$ amu. The identity of the $HfFCl_2^+$ ion was confirmed based on its characteristic Hf and Cl isotopes. The calculated mass spectrum was generated based upon the natural Hf and Cl isotopes. The calculated spectrum in Figure 6 shows excellent agreement with the QMS spectrum.

The $HfFCl_2^+$ ion may be a fragment of the parent $HfFCl_3^+$ molecular ion. This parent $HfFCl_3^+$ molecular ion was observed by a cluster of mass intensities with the highest
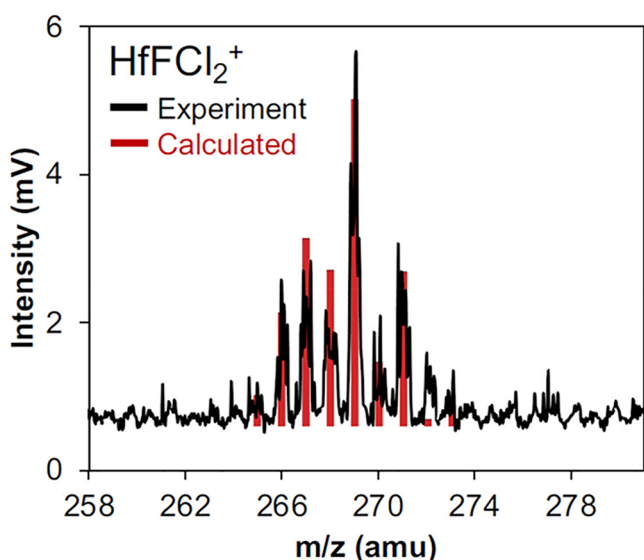
Figure 6. Mass spectrum showing ion signals for $HfFCl_2^+$ during reaction between $SiCl_4$ and HfF_4 powder at 523 °C.

Figure 7. Ion signal intensities of (a) precursor ($SiCl_3^+$) and precursor after ligand exchange (SiF_3^+ and $SiFCl_3^+$) and (b) Hf-containing etch products versus powder temperature during reaction between $SiCl_4$ and HfF_4 powder. The most intense isotope peak of each species was employed in the plots.

peak intensity at m/z = 304 amu. The ion from the fully chlorinated etch product, $HfCl_4$, was also observed in the mass spectrum with the highest peak intensity at m/z = 320 amu. The presence of $HfCl_4^+$ indicates that the ligand-exchange reaction can proceed to replace all four fluorine ligands on HfF_4 with Cl atoms.

The temperature dependence of the ligand-exchange reaction between $SiCl_4$ and HfF_4 powder is shown in Figure 7. The $SiCl_3^+$ signal with its highest intensity peak at m/z = 135 amu is the prominent fragment of the $SiCl_4$ precursor. Figure 7a indicates that the $SiCl_3^+$ signal intensity decreases progressively with increasing temperature. Initially, there are no identifiable ligand-exchange products that correlate with the decrease of the $SiCl_3^+$ signal intensity. However, the SiF_3^+ intensity with its highest intensity peak at m/z = 85 amu starts to rise at 200 °C. The SiF_3^+ intensity is the prominent fragment of the SiF_4 ligand-exchange product.

Above 200 °C, there is complementary behavior between the intensity changes of the $SiCl_4$ precursor and SiF_4 ligand-exchange product. These results argue that ligand exchange can proceed fully to form SiF_4 from $SiCl_4$. This observation suggests that multiple ligand exchanges are more favorable than a single ligand exchange. These results argue that the $SiCl_4$ precursor has sufficient residence time on the surface and in the HfF_4 powder to undergo multiple ligand-exchange reactions with the HfF_4 surface.

Another interesting feature in Figure 7a is the correlation between the peak of the SiF_3^+ intensity and minimum in the $SiCl_3^+$ intensity around 340 °C. During the continued temperature ramp, the inverse correlation can be observed by the peak in the $SiCl_3^+$ intensity and the corresponding minimum in the SiF_3^+ intensity around 400 °C. The $SiCl_3^+$ intensity then decreases and the SiF_3^+ intensity increases above 400 °C. These correlations clearly establish the complementary behavior between $SiCl_4$ precursor loss and SiF_4 product gain versus temperature. Perhaps some of this complementary behavior is associated with the residence time of the $SiCl_4$ precursor on the HfF_4 surface and the kinetics of the ligand-exchange reaction. Higher temperatures would lower the residence time of the $SiCl_4$ precursor[32−34] and provide thermal
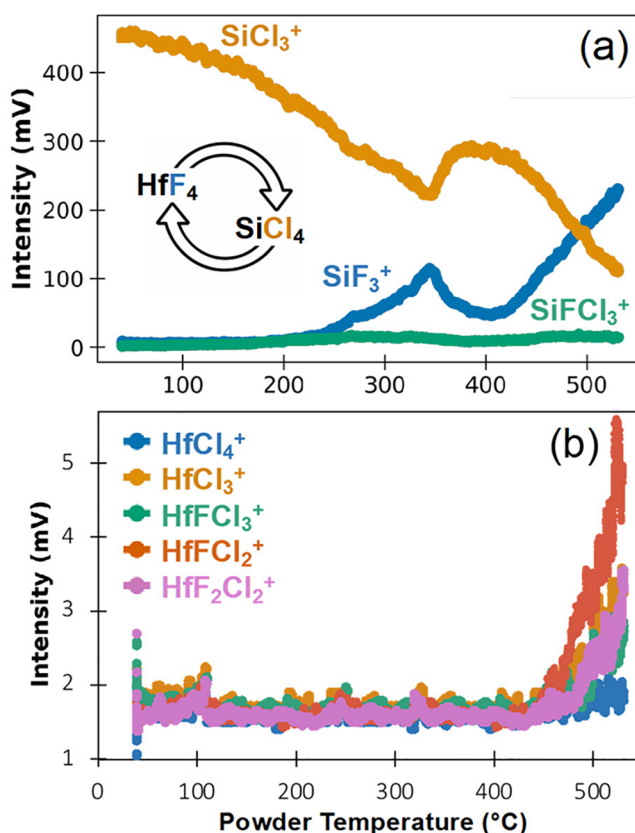
energy to overcome activation barriers for the ligand-exchange reaction.

Figure 7b also shows that volatile Hf-containing etch products were not observed until the sample temperature exceeded 450 °C. Comparison between the Si ligand-exchange products and the Hf-containing etch products reveals that ligand exchange can occur at low temperature, but the Hf-containing etch products are not observed until much higher temperatures. $HfCl_4$ has a vapor pressure of 6 Torr at 203 °C and 1214 Torr at 329 °C.[35,36] However, the Hf-containing etch products are not detected until >450 °C, above the melting point of $HfCl_4$ at 432 °C. If $HfCl_4$ was formed on the surface, then $HfCl_4$ should be volatilized at temperatures much lower than 450 °C.

The discrepancy between the relatively high $HfCl_4$ vapor pressure at temperatures below 450 °C and the lack of Hf-containing etch products until temperatures >450 °C suggests that $HfCl_4$ was not formed until the temperatures exceeded 450 °C. Given that the ligand-exchange reaction was occurring at temperatures >250 °C based on the increase of the SiF_3^+ signal intensity, Cl must be building up in the HfF_4 film. Sufficient Cl must have built up in the HfF_4 film to yield $HfCl_4$ and other HfF_xCl_y species at temperatures >450 °C.

Figure 7 paints a key picture for describing the landscape of spontaneous etching by ligand-exchange reactions. The presence of ligand-exchange products does not always equate with the formation of volatile metal etch products from the substrate. Ligand-exchange reactions and volatilization of metal

etch products from the substrate do not always occur concurrently. Ligand exchange can occur over a wide temperature range before the metal etch products from the substrate are observed at higher temperatures.

III.C. SiCl$_4$ + InF$_3$. The volatile etch products formed during the spontaneous etching of InF$_3$ powder by SiCl$_4$ were examined by *in situ* QMS studies. This system is not related to previous thermal ALE studies. However, the results of this investigation could be predictive of In$_2$O$_3$ thermal ALE using HF and SiCl$_4$ as the reactants. The exposure of SiCl$_4$ to InF$_3$ powder at 335 °C yielded several In-containing etch products. The intensities of the InCl$_2^+$, InCl$_3^+$, and In$_2$Cl$_5^+$ ions are shown in Figure 8. InCl$_2^+$ is observed with the highest intensity peak at m/z = 185 amu in Figure 8a. InCl$_2^+$ is believed to originate from the InCl$_3$ parent. The observation of InCl$_3^+$ with

the highest peak intensity at m/z = 220 amu in Figure 8b confirms the presence of InCl$_3$. The InCl$_3^+$ ion is consistent with the full ligand exchange of InF$_3$ to InCl$_3$. The observed signals for InCl$_2^+$ and InCl$_3^+$ are consistent with the expected intensities based on the isotopic abundances.

The presence of In$_2$Cl$_5^+$ shown in Figure 8c with its highest intensity peak at m/z = 407 amu reveals that In dimers are also etch products. In$_2$Cl$_5^+$ is believed to originate from the loss of one Cl during the electron-impact ionization of the In$_2$Cl$_6$ dimer. In$_2$Cl$_5^+$ could be analogous to superhalogen clusters that have been reported with a stoichiometry of Mn$_x$Cl$_{2x+1}$.[37] The identification of the In$_2$Cl$_5^+$ ion is also consistent with the expected signals based on the Cl and In isotopic abundances.

The temperature dependence of the ion intensities during the SiCl$_4$ + InF$_3$ ligand-exchange reaction is shown in Figure 9.

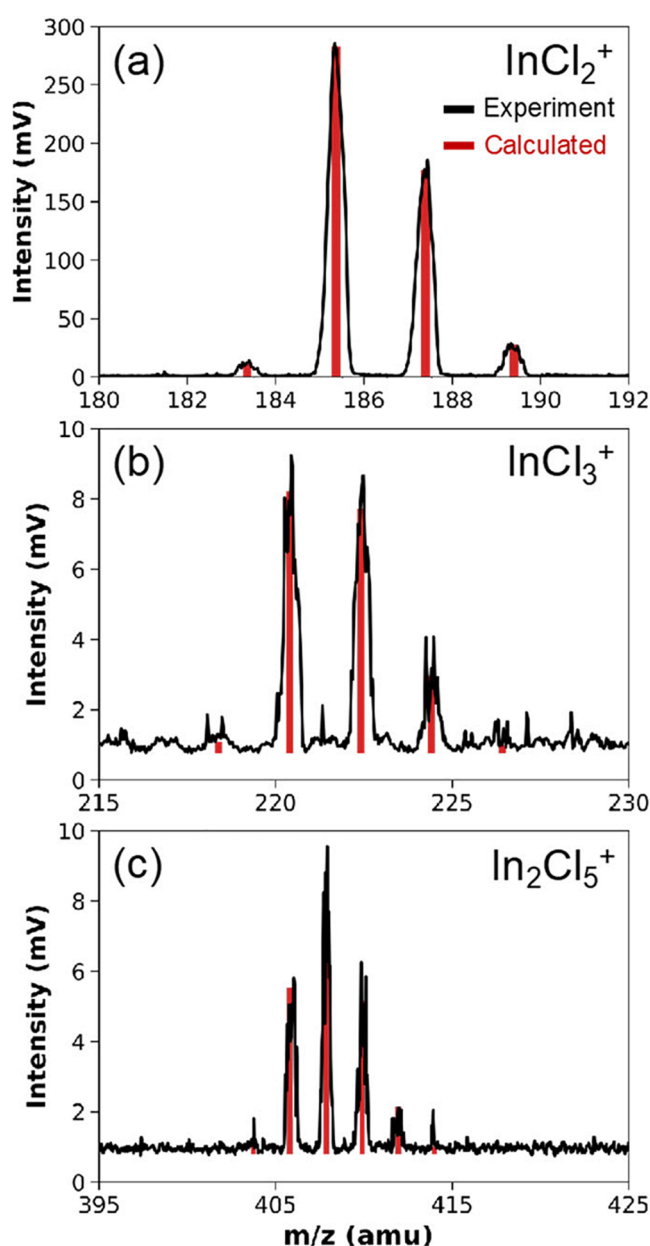**Figure 8.** Mass spectra showing In-containing etch products observed by ion signals for (a) InCl$_2^+$, (b) InCl$_3^+$, and (c) In$_2$Cl$_5^+$ during reaction between SiCl$_4$ and InF$_3$ powder at 335 °C.
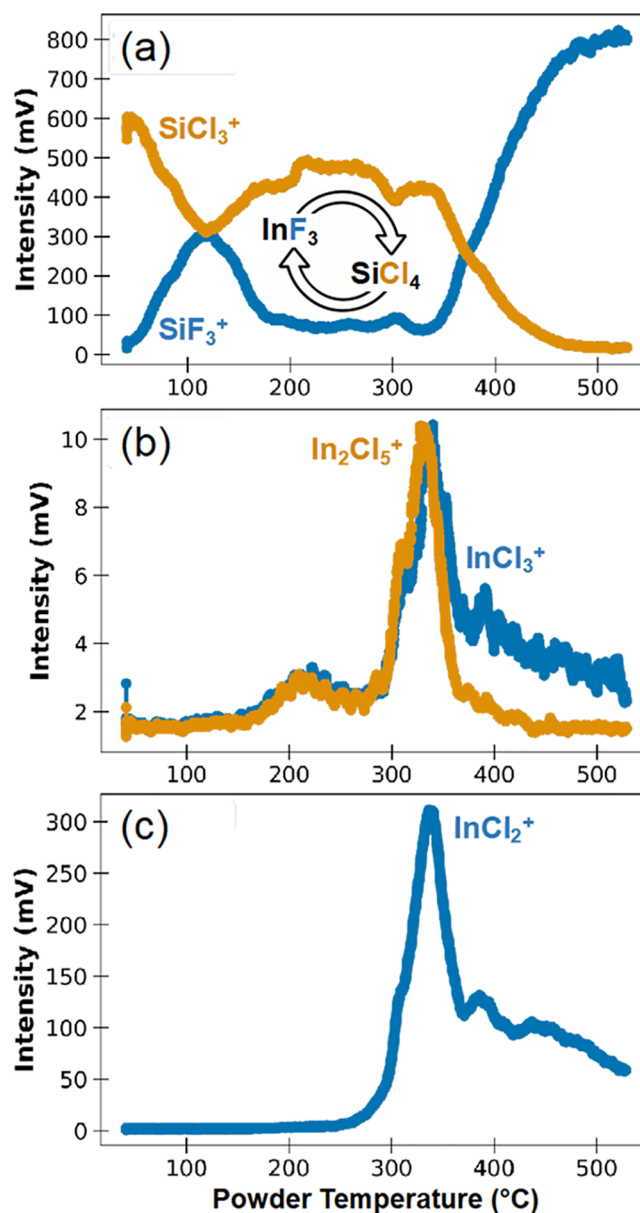

Figure 9. Ion signal intensities for (a) precursor (SiCl$_3^+$) and precursor after ligand exchange (SiF$_3^+$ and SiFCl$_3^+$), (b) InCl$_3^+$ and In$_2$Cl$_5^+$, and (c) InCl$_2^+$ versus powder temperature during reaction between SiCl$_4$ and InF$_3$ powder. The most intense isotope peak of each species was employed in the plots.

Similar to the results in Figure 7a, the intensities for the $SiCl_3^+$ ion from $SiCl_4$ with its highest intensity at $m/z = 135$ amu and the SiF_3^+ ion from the SiF_4 ligand-exchange product with its highest intensity at $m/z = 85$ amu exhibit complementary signal intensities during the temperature ramp.

The $SiCl_3^+$ intensity decreases as the SiF_3^+ intensity increases between 25 and 125 °C. The $SiCl_3^+$ intensity then increases as the SiF_3^+ intensity decreases between 125 and 200 °C. The $SiCl_3^+$ and SiF_3^+ intensities are roughly constant between 200 and 330 °C. Subsequently, the $SiCl_3^+$ intensity decreases as the SiF_3^+ intensity increases between 330 and 450 °C. This complementary behavior indicates that the efficiency of the ligand-exchange reaction changes versus temperature.

Figure 9b,c shows that the intensities for $InCl_2^+$, $InCl_3^+$, and $In_2Cl_5^+$ increase suddenly at 300 °C and reach a peak at 330 °C. As the $InCl_3$ and In_2Cl_6 etch products are desorbed from the surface, more InF_3 becomes accessible. The $SiCl_4$ precursor can again undergo ligand exchange with the fresh InF_3 surface. Consequently, the $SiCl_3^+$ intensity decreases as the SiF_3^+ intensity increases between 330 and 450 °C.

The ligand-exchange reactions between $SiCl_4$ and InF_3 are observed below 100 °C in Figure 9a. However, the In-containing etch products are not detected until the sample temperature exceeded 300 °C as shown in Figure 9b,c. Cl−F ligand-exchange products are formed at low temperature. However, the low temperatures are not sufficient for volatilization of In-containing species. There must be a buildup of $InCl_x$ etch products on the surface at low temperature. Temperatures greater than 300 °C are required for the desorption of the $InCl_3$ etch products. In support of this interpretation, the reported vapor pressure of $InCl_3$ is 0.18 Torr at 330 °C.[38]

III.D. $TiCl_4$ + SnF_4. *In situ* QMS studies were also employed to examine the spontaneous etching of SnF_4 powder by $TiCl_4$. This system is exploratory and is not connected to any previous thermal ALE study. The observation of volatile etch products could predict the feasibility of SnO_2 thermal ALE using HF and $TiCl_4$ as the reactants. The exposure of $TiCl_4$ to SnF_4 powder produced various Sn-containing etch products. Figure 10 shows the $SnCl_4^+$ and $SnFCl_3^+$ ion signals that are observed at 260 and 330 °C, respectively. $SnCl_4^+$ is observed with the highest intensity peak at $m/z = 260$ amu. $SnCl_4$ is the result of four F−Cl ligand-exchange reactions. $SnFCl_3^+$ is also observed with the highest intensity peak at $m/z = 244$ amu. $SnFCl_3$ is the result of three Cl−F ligand-exchange reactions. The Sn and Cl isotopes allow these products to be readily identifiable.

Different degrees of ligand exchange were also observed for the $TiCl_4$ precursor. Figure 11 shows the various $TiF_xCl_y^+$ ion species resulting from ligand-exchange reactions at 165 °C. $TiFCl_3^+$ with its highest intensity peak at $m/z = 172$ amu in Figure 11a results from one F−Cl ligand exchange. $TiF_2Cl_2^+$ in Figure 11b with its highest intensity peak at $m/z = 156$ amu results from two ligand exchanges. TiF_3Cl^+ in Figure 11c with its highest intensity peak at $m/z = 140$ amu results from three ligand exchanges. The possible TiF_4^+ ion that should be observed at $m/z = 124$ amu was difficult to detect because of overlap with one of the Sn isotopes. However, TiF_3^+ was observed with its highest intensity peak at $m/z = 105$ amu. TiF_3^+ could be a fragment of TiF_3Cl or TiF_4.

The change of the ion intensities during the $TiCl_4$ + SnF_4 reaction versus temperature is displayed in Figure 12. Ion intensities from the various TiF_xCl_y ligand-exchange products
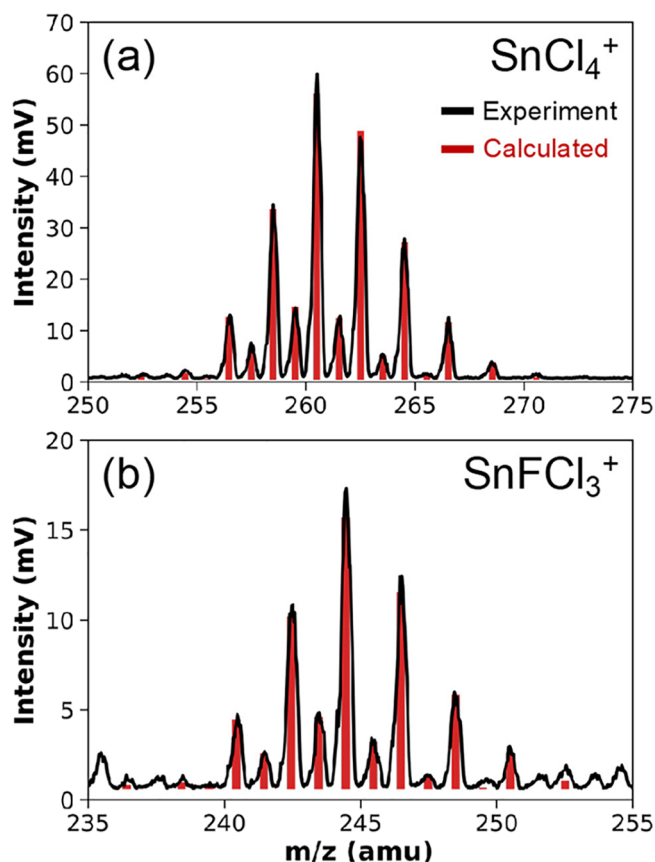

Figure 10. Mass spectra showing ion signals for etch products (a) $SnCl_4^+$ at 260 °C and (b) $SnFCl_3^+$ at 330 °C observed during reaction between $TiCl_4$ and SnF_4 powder.

from the $TiCl_4$ + SnF_4 reaction are displayed in Figure 12a. The $TiFCl_3^+$ ion in Figure 12a from the ligand-exchange reaction shows some complementary behavior with the $TiCl_4^+$ ion from the $TiCl_4$ precursor with its highest intensity at $m/z = 190$ amu. The $TiFCl_3^+$ ion intensity increases from 75 to 165 °C as the $TiCl_4^+$ ion intensity decreases from 75 to 165 °C. The $TiF_2Cl_2^+$ ion appears to have signal intensity at the beginning of the heat ramp at 18 °C. However, some of the ion intensity at $m/z = 156$ amu assigned to $TiF_2Cl_2^+$ may also result from $TiCl_3^+$ from the $TiCl_4$ precursor.

The $TiFCl_3^+$ ion intensity in Figure 12a shows some complementary behavior with the $TiCl_4^+$ ion intensity. The $TiFCl_3^+$ intensity increases from 75 to 165 °C as the $TiCl_4^+$ intensity decreases from 75 to 165 °C. In addition, the $TiF_2Cl_2^+$ ion signal also exhibits complementary behavior with the $TiCl_4^+$ ion intensity and increases from 125 to 195 °C. The TiF_3Cl^+ ion intensity also is complementary with the $TiCl_4^+$ ion intensity. The TiF_3Cl^+ intensity increases from 165 to 225 °C as the $TiCl_4^+$ intensity continues to decrease from 165 to 225 °C.

The various SnF_xCl_y etch products from the $TiCl_4$ + SnF_4 reaction are displayed in Figure 12b. The $SnCl_4^+$ ion intensity from the $SnCl_4$ etch product with its highest intensity at $m/z = 260$ amu is observed at low temperature with an onset at 125 °C. The low starting temperature for the appearance of $SnCl_4$ suggests that the ligand-exchange reactions are very efficient between $TiCl_4$ and SnF_4. $TiCl_4$ can readily complete four Cl/F ligand exchanges with SnF_4 to form $SnCl_4$. The $SnCl_4$ etch product can then desorb because $SnCl_4$ is a fuming liquid with
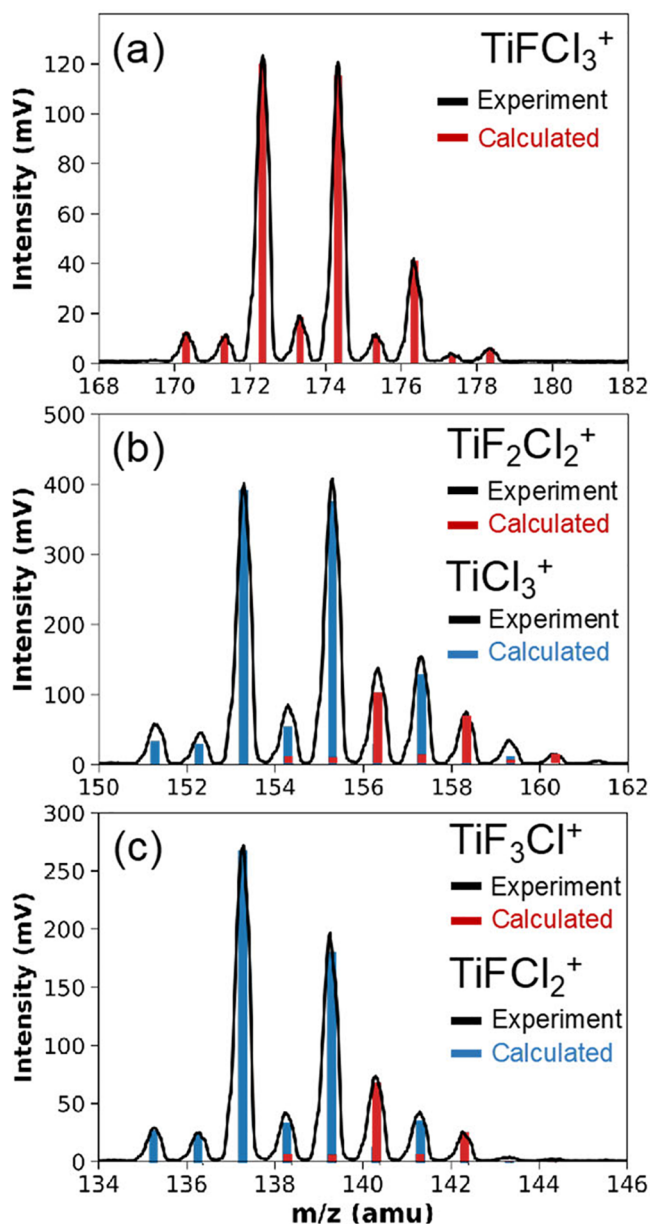
Figure 11. Mass spectra showing ion signals for ligand-exchange products (a) $TiFCl_3^+$, (b) $TiF_2Cl_2^+$, and (c) TiF_3Cl^+ observed during reaction between $TiCl_4$ and SnF_4 powder at 165 °C.

Figure 12. Ion signal intensities of (a) precursor ($TiCl_4^+$) and precursor after ligand exchange ($TiFCl_3^+$, $TiF_2Cl_2^+$, and TiF_3Cl^+) and (b) Sn etch products observed by $SnCl_4^+$ and $SnFCl_3^+$ versus powder temperature during reaction between $TiCl_4$ and SnF_4 powder. The most intense isotope peak of each species was employed in the plots.

a vapor pressure of 26 Torr at room temperature and 760 Torr at 113 °C.[39,40] These results suggest that SnO_2 thermal ALE should be possible using HF for fluorination and $TiCl_4$ for ligand exchange at relatively low temperatures of ≥125 °C.

The spontaneous etching of SnF_4 powder by $TiCl_4$ is an example of a system where the metal etch products appear at temperatures very similar to the temperatures for the ligand-exchange products. The $SnCl_4$ etch product does not build up and appear at much higher temperatures than the temperatures for the ligand-exchange products. The $TiCl_4$ + SnF_4 system adds to the diverse landscape of spontaneous etching by ligand exchange. This important class of etching results from ligand-exchange reactions where the ligand exchange and release of metal etch products occur at nearly the same temperature.

Another interesting feature in Figure 12b is the $SnFCl_3^+$ ion intensity from the $SnFCl_3$ etch product with its highest intensity peak at $m/z = 244$ amu. The $SnFCl_3^+$ intensity is not
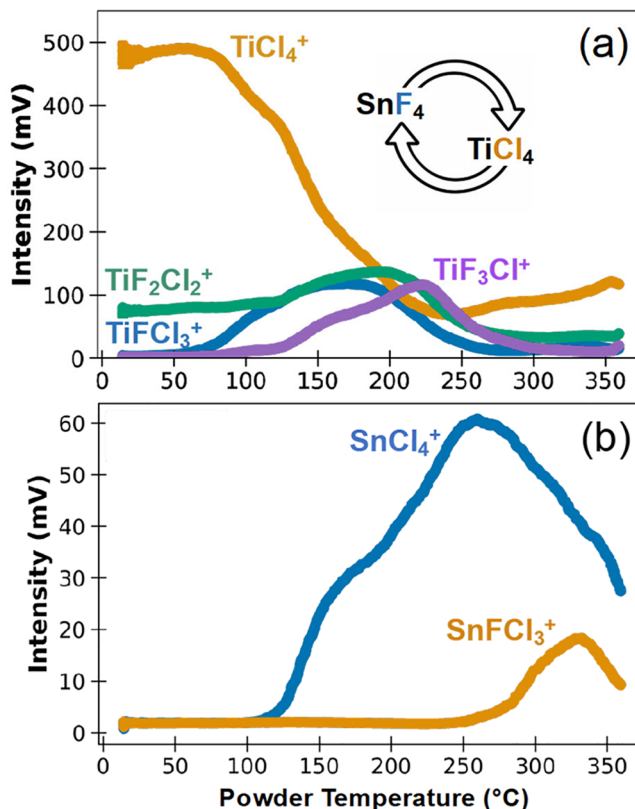
observed until much higher temperatures with an onset around 280 °C. The increase of the $SnFCl_3^+$ intensity coincides with the decrease of the $SnCl_4^+$ intensity. This correlation suggests that the $SnFCl_3$ etch product becomes dominant at higher temperatures. The $SnCl_4$ etch product will no longer be observed if $SnFCl_3$ can desorb from the surface prior to the formation of $SnCl_4$.

III.E. Al(CH$_3$)$_3$ + GaF$_3$. Previous quartz crystal microbalance studies demonstrated Ga_2O_3 thermal ALE using HF and TMA as the reactants.[9] During Ga_2O_3 thermal ALE, HF is believed to fluorinate Ga_2O_3 to form GaF_3. TMA can then undergo ligand exchange with GaF_3 to yield volatile Ga etch products.[9] *In situ* QMS measurements were performed in this study to identify the ligand-exchange products during the reaction of TMA with GaF_3. Figure 13a shows that the reaction of TMA with GaF_3 at 250 °C produces strong ion intensities for $Ga(CH_3)_2^+$ at $m/z = 99$ amu and $m/z = 101$ amu resulting from the ^{69}Ga and ^{71}Ga isotopes at relative abundances of 60% and 40%, respectively. $Ga(CH_3)_2^+$ is the main fragment resulting from the electron impact ionization of $Ga(CH_3)_3$.[41]

The products during the reaction of TMA with GaF_3 also illustrate the rich ligand-exchange possibilities for the TMA precursor. Figure 13b shows the variety of $AlF_x(CH_3)_y^+$ species that were observed resulting from the reaction of TMA with GaF_3 at 250 °C. $Al_2F(CH_3)_4^+$ is observed at $m/z = 133$ amu. $Al_2F_2(CH_3)_3^+$ is detected at $m/z = 137$ amu. In addition, $Al_3F_3(CH_3)_5^+$ is monitored at $m/z = 213$ amu. These ion signals were also observed for the reaction of TMA with AlF_3 in Figure 4. In addition, the reaction of TMA with GaF_3
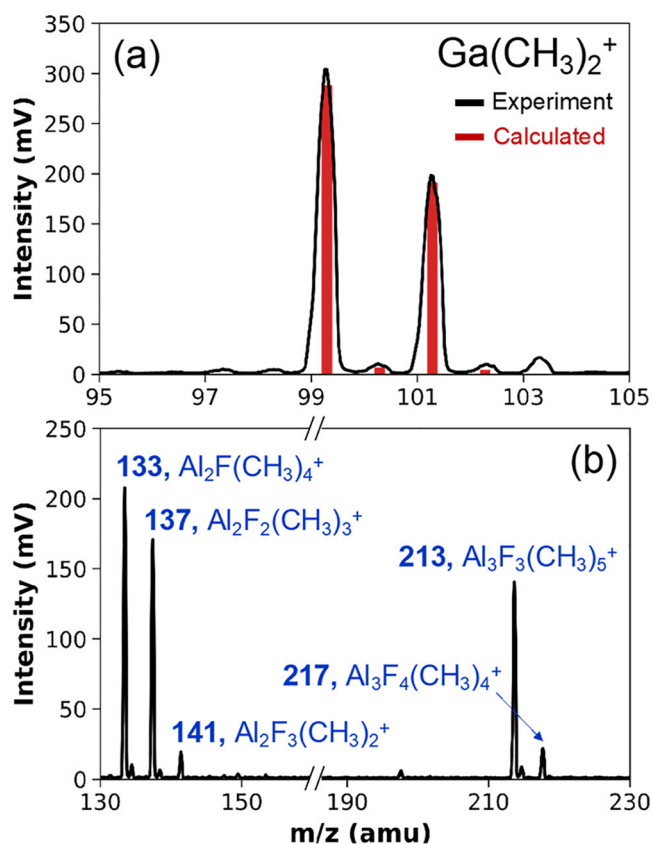
Figure 13. Mass spectra showing ion signals for (a) $Ga(CH_3)_2^+$ and (b) Al etch products observed by dimers and trimers during reaction between $Al(CH_3)_3$ and GaF_3 powder at 250 °C.

Figure 14. Ion signal intensities of (a) precursor ($SiCl_3^+$) and precursor after ligand exchange (SiF_3^+) and (b) absence of any Al etch products versus powder temperature during interaction between $SiCl_4$ and AlF_3 powder. The most intense isotope peak of each species was employed in the plots.

yielded an Al dimer identified as $Al_2F_3(CH_3)_2^+$ at $m/z = 141$ amu and an Al trimer assigned to $Al_3F_4(CH_3)_4^+$ at $m/z = 217$ amu.

For the ligand-exchange reaction between TMA and AlF_3, the Al dimers and trimers observed in Figure 4 could have originated from Al in the TMA precursor or in the AlF_3 substrate. In contrast, for the ligand-exchange reaction between TMA and GaF_3, the Al dimers and trimers must contain Al from the TMA precursor. The observation of dimers and trimers of Al indicates that the TMA precursor and the DMAF from the ligand-exchange reaction can bind with each other. These results illustrate the rich possibilities during ligand-exchange reactions. There can be dimerization or trimerization of the Al etch products that originate from the AlF_3 surface. Likewise, there also can be dimerization or trimerization of the TMA precursor with the DMAF products from the ligand exchange. The formation of these Al dimers and trimers presumably requires a sufficient residence time of TMA and DMAF on the surface.

III.F. SiCl₄ + AlF₃. The reaction of $SiCl_4$ with AlF_3 was also studied using *in situ* QMS characterization. The ligand-exchange reaction between $SiCl_4$ and AlF_3 does not lead to etching because Al_2O_3 thermal ALE was not observed using HF and $SiCl_4$ as the reactants.[28] Figure 14a shows the results for the ion intensities of $SiCl_3^+$ with its highest intensity at $m/z = 135$ amu and SiF_3^+ with its highest intensity at $m/z = 85$ amu during the reaction of $SiCl_4$ with AlF_3 powder. These results suggest that there is facile ligand exchange that converts the $SiCl_4$ precursor to SiF_4 product after four Cl/F ligand-exchange reactions. There is also complementary behavior
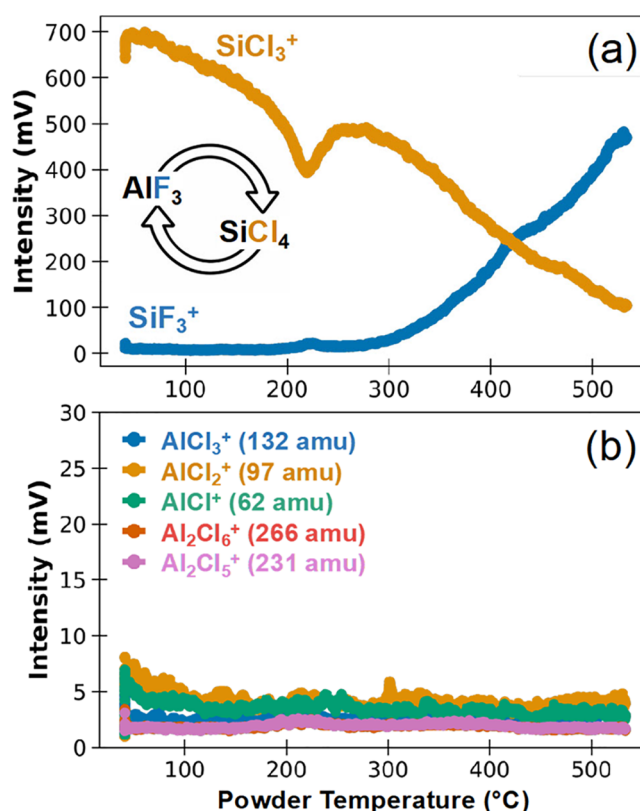
between the $SiCl_3^+$ and SiF_3^+ ion intensities. The decrease of the ion intensity for $SiCl_3^+$ is correlated with the increase of the ion intensity of SiF_3^+ for temperatures above 200 °C.

Although the SiF_3^+ ion resulting from ligand-exchange reactions is clearly detected in Figure 14a, no $Al_xCl_y^+$ ion species from the AlF_3 substrate were observed in Figure 14b up to 530 °C. These results illustrate that even when ligand-exchange reactions can occur, they do not necessarily result in volatile metal etch products from the substrate. These results are consistent with thermochemical considerations,[28] previous etching results,[28] and earlier *in situ* QMS results.[23] Thermochemical calculations for the ligand-exchange reaction between $SiCl_4$ and AlF_3 yield a positive change in the Gibbs Free Energy for temperatures from 0 to 500 °C.[28] No Al_2O_3 thermal ALE was observed using HF and $SiCl_4$ as the reactants at 350 °C.[28] Previous *in situ* QMS results of the reaction of $SiCl_4$ with AlF_3 powder at 300 °C also observed $SiF_xCl_y^+$ ion species from the ligand-exchange reaction with no Al-containing etch products from the AlF_3 substrate.[23]

IV. LANDSCAPE OF SPONTANEOUS ETCHING VIA LIGAND EXCHANGE

A landscape of spontaneous etching using the ligand-exchange reaction can be established from the case studies discussed above:

First, the occurrence of the ligand-exchange products and the metal etch products can be at separate temperatures. This landscape is illustrated in Figure 15a. Examples of this scenario include $SiCl_4$ + HfF_4 and $SiCl_4$ + InF_3. The ligand-exchange
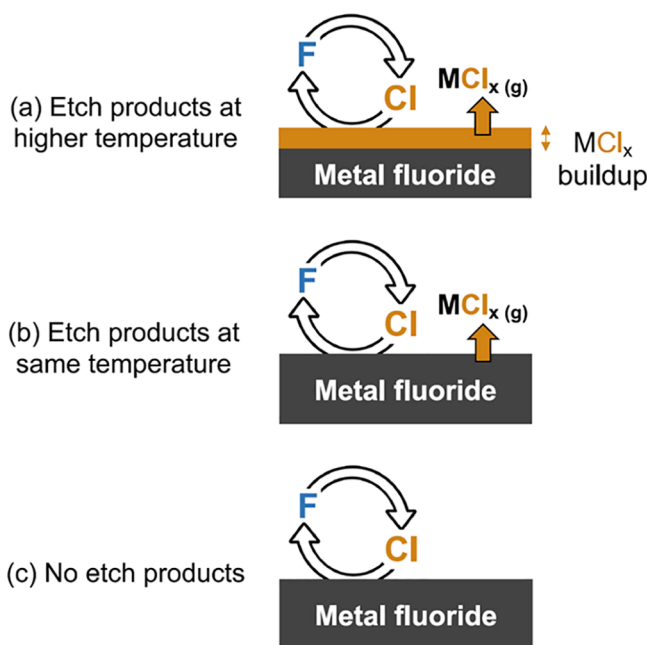
Figure 15. Schematic showing landscape observed during spontaneous etching: (a) ligand exchange occurs at low temperature, but metal etch products from the substrate require buildup and are not observed until high temperature; (b) ligand-exchange and metal etch products from the substrate are observed at similar temperature; and (c) ligand exchange occurs but no metal etch products from the substrate are observed up to limiting high temperature.

product, SiF_3^+, was observed at lower temperatures. However, the Hf- and In-containing metal etch products were not observed until higher temperatures. During this type of spontaneous etching, the F/Cl ligand exchange can occur at lower temperatures. The metal chloride etch products require higher temperatures to form and/or desorb from the surface.

Second, the observation of the ligand-exchange products and the metal etch products can be at a similar temperature. This class of landscape is depicted in Figure 15b. Examples of this scenario are $Al(CH_3)_3$ + AlF_3 and $TiCl_4$ + SnF_4. During this type of spontaneous etching, the ligand exchange leads to metal etch products that thermally desorb at the same temperatures. There is no buildup because the metal etch products form and are not desorption-limited.

Third, the ligand-exchange products can be observed with no appearance of metal etch products even at high temperature. This landscape is portrayed in Figure 15c. An example of this scenario is $SiCl_4$ + AlF_3. The observation of ligand exchange does not necessarily equate to the formation of metal etch products. Ligand exchange can still occur even in the absence of etching. These results with no observable etch products are supported by the unfavorable thermochemistry of the overall etching reaction.

V. CONCLUSIONS

The volatile etch products from the reaction of ligand-exchange precursors with metal fluoride powders were studied using a new reactor equipped with *in situ* QMS. The experiments used molecular beam techniques to improve the detection sensitivity and reduce possible wall effects. The *in situ* QMS studies tracked the various ligand-exchange products and the volatile metal etch products from the substrate versus temperature. AlF_3, HfF_4, GaF_3, InF_3, and SnF_4 were explored

as metal fluoride powders. $Al(CH_3)_3$, $SiCl_4$, and $TiCl_4$ were utilized as ligand-exchange precursors.

Various categories of behavior were observed by the temperature-dependent studies. (i) For $SiCl_4$ + HfF_4 and $SiCl_4$ + InF_3, ligand exchange occurred at low temperature, but metal etch products from the substrate were not observed until higher temperature. (ii) For $Al(CH_3)_3$ + AlF_3 and $TiCl_4$ + SnF_4, ligand-exchange and metal etch products from the substrate were observed at similar temperatures. (iii) For $SiCl_4$ + AlF_3, ligand-exchange occurred, but no metal etch products from the substrate were observed up to a limiting temperature. These temperature-dependent *in situ* QMS studies revealed the many possibilities that can occur during reactions between ligand-exchange precursors and metal fluoride powders.

The studies on $Al(CH_3)_3$ + AlF_3, $SiCl_4$ + HfF_4, and $Al(CH_3)_3$ + GaF_3 provided insight for thermal Al_2O_3 ALE using HF and TMA, thermal HfO_2 ALE using HF and $SiCl_4$, and thermal Ga_2O_3 ALE using HF and TMA, respectively. Ligand-exchange products and metal etch products from the substrate were observed for all of these systems. The studies on $SiCl_4$ + InF_3 and $TiCl_4$ + SnF_4 also observed ligand-exchange products and metal etch products from the substrate that are predictive of the thermal ALE of In_2O_3 and SnO_2 using HF and either $SiCl_4$ or $TiCl_4$ as the reactants. The study on $SiCl_4$ + AlF_3 observed ligand-exchange products but no metal etch products from the substrate. These results are consistent with earlier investigations that reported no occurrence of thermal Al_2O_3 ALE with HF and $SiCl_4$ as the reactants.

The *in situ* QMS studies of ligand-exchange precursors and metal fluoride powders revealed the wide range of possibilities of spontaneous etching. These studies of spontaneous etching can also serve as predictors for thermal ALE of new materials assuming that the initial metal oxide or metal nitride can be fluorinated to the metal fluoride. Identifying etch products is instrumental for designing chemistries for selective spontaneous etching. Furthermore, etch selectivity could be derived based on the different onset temperatures for various etching reactions. There is also a richness in the reactions for both the ligand-exchange precursors and the metal fluorides as revealed by the TMA + GaF_3 system. Understanding the various possibilities for reactions between ligand-exchange precursors and metal fluoride powders enables a more complete comprehension of thermal ALE.

ASSOCIATED CONTENT

Supporting Information

The Supporting Information is available free of charge at https://pubs.acs.org/doi/10.1021/acs.chemmater.1c01950.

> Additional experimental details for the reactor, sample housing and heating, molecular beam generation and skimmer, quadrupole mass spectrometer, and ligand-exchange experiments (PDF)

AUTHOR INFORMATION

Corresponding Author

Steven M. George − *Department of Chemistry, University of Colorado, Boulder, Colorado 80309, United States;*
 orcid.org/0000-0003-0253-9184;
Email: steven.george@colorado.edu

Authors

Ann Lii-Rosales − *Department of Chemistry, University of Colorado, Boulder, Colorado 80309, United States*

Andrew S. Cavanagh − *Department of Chemistry, University of Colorado, Boulder, Colorado 80309, United States;* ● orcid.org/0000-0002-6201-530X

Andreas Fischer − *Lam Research Corporation, Fremont, California 94538, United States*

Thorsten Lill − *Lam Research Corporation, Fremont, California 94538, United States*

Complete contact information is available at:
https://pubs.acs.org/10.1021/acs.chemmater.1c01950

Notes

The authors declare no competing financial interest.

■ REFERENCES

(1) George, S. M. Mechanisms of Thermal Atomic Layer Etching. *Acc. Chem. Res.* **2020**, *53*, 1151−1160.

(2) Lee, Y.; George, S. M. Atomic Layer Etching of Al_2O_3 Using Sequential, Self-Limiting Thermal Reactions with $Sn(acac)_2$ and Hydrogen Fluoride. *ACS Nano* **2015**, *9*, 2061−2070.

(3) Fischer, A.; Routzahn, A.; George, S. M.; Lill, T. Thermal Atomic Layer Etching: A Review. *J. Vac. Sci. Technol., A* **2021**, *39*, 030801.

(4) Lee, Y.; DuMont, J. W.; George, S. M. Trimethylaluminum as the Metal Precursor for the Atomic Layer Etching of Al_2O_3 Using Sequential, Self-Limiting Thermal Reactions. *Chem. Mater.* **2016**, *28*, 2994−3003.

(5) Lee, Y.; George, S. M. Thermal Atomic Layer Etching of Al_2O_3, HfO_2, and ZrO_2 Using Sequential Hydrogen Fluoride and Dimethylaluminum Chloride Exposures. *J. Phys. Chem. C* **2019**, *123*, 18455−18466.

(6) Lee, Y.; DuMont, J. W.; George, S. M. Atomic Layer Etching of HfO_2 Using Sequential, Self-Limiting Thermal Reactions with $Sn(acac)_2$ and HF. *ECS J. Solid State Sci. Technol.* **2015**, *4*, N5013−N5022.

(7) Lee, Y.; George, S. M. Thermal Atomic Layer Etching of HfO_2 using HF for Fluorination and $TiCl_4$ for Ligand-Exchange. *J. Vac. Sci. Technol., A* **2018**, *36*, 061504.

(8) Zywotko, D. R.; George, S. M. Thermal Atomic Layer Etching of ZnO by a "Conversion-Etch" Mechanism Using Sequential Exposures of Hydrogen Fluoride and Trimethylaluminum. *Chem. Mater.* **2017**, *29*, 1183−1191.

(9) Lee, Y.; Johnson, N. R.; George, S. M. Thermal Atomic Layer Etching of Gallium Oxide Using Sequential Exposures of HF and Various Metal Precursors. *Chem. Mater.* **2020**, *32*, 5937−5948.

(10) Johnson, N. R.; George, S. M. WO_3 and W Thermal Atomic Layer Etching Using "Conversion-Fluorination" and "Oxidation-Conversion-Fluorination" Mechanisms. *ACS Appl. Mater. Interfaces* **2017**, *9*, 34435−34447.

(11) Johnson, N. R.; Sun, H. X.; Sharma, K.; George, S. M. Thermal Atomic Layer Etching of Crystalline Aluminum Nitride Using Sequential, Self-limiting Hydrogen Fluoride and $Sn(acac)_2$ Reactions and Enhancement by H_2 and Ar Plasmas. *J. Vac. Sci. Technol., A* **2016**, *34*, 050603.

(12) Lee, Y.; George, S. M. Thermal Atomic Layer Etching of Titanium Nitride Using Sequential, Self-Limiting Reactions: Oxidation to TiO_2 and Fluorination to Volatile TiF_4. *Chem. Mater.* **2017**, *29*, 8202−8210.

(13) Johnson, N. R.; Hite, J. K.; Mastro, M. A.; Eddy, C. R.; George, S. M. Thermal Atomic Layer Etching of Crystalline GaN Using Sequential Exposures of XeF_2 and BCl_3. *Appl. Phys. Lett.* **2019**, *114*, 243103.

(14) Abdulagatov, A. I.; George, S. M. Thermal Atomic Layer Etching of Silicon Using O_2, HF, and $Al(CH_3)_3$ as the Reactants. *Chem. Mater.* **2018**, *30*, 8465−8475.

(15) DuMont, J. W.; Marquardt, A. E.; Cano, A. M.; George, S. M. Thermal Atomic Layer Etching of SiO_2 by a "Conversion-Etch" Mechanism Using Sequential Reactions of Trimethylaluminum and Hydrogen Fluoride. *ACS Appl. Mater. Interfaces* **2017**, *9*, 10296−10307.

(16) Abdulagatov, A. I.; George, S. M. Thermal atomic layer etching of silicon nitride using an oxidation and "conversion etch" mechanism. *J. Vac. Sci. Technol., A* **2020**, *38*, 022607.

(17) Mohimi, E.; Chu, X. Q. I.; Trinh, B. B.; Babar, S.; Girolami, G. S.; Abelson, J. R. Thermal Atomic Layer Etching of Copper by Sequential Steps Involving Oxidation and Exposure to Hexafluoroacetylacetone. *ECS J. Solid State Sci. Technol.* **2018**, *7*, P491−P495.

(18) Konh, M.; He, C.; Lin, X.; Guo, X. Y.; Pallem, V.; Opila, R. L.; Teplyakov, A. V.; Wang, Z. J.; Yuan, B. Molecular Mechanisms of Atomic Layer Etching of Cobalt with Sequential Exposure to Molecular Chlorine and Diketones. *J. Vac. Sci. Technol., A* **2019**, *37*, 021004.

(19) Carver, C. T.; Plombon, J. J.; Romero, P. E.; Suri, S.; Tronic, T. A.; Turkot, R. B. Atomic Layer Etching: An Industry Perspective. *ECS J. Solid State Sci. Technol.* **2015**, *4*, N5005−N5009.

(20) Cano, A. M.; Marquardt, A. E.; DuMont, J. W.; George, S. M. Effect of HF Pressure on Thermal Al_2O_3 Atomic Layer Etch Rates and Al_2O_3 Fluorination. *J. Phys. Chem. C* **2019**, *123*, 10346−10355.

(21) Kondati Natarajan, S.; Elliott, S. D. Modeling the Chemical Mechanism of the Thermal Atomic Layer Etch of Aluminum Oxide: A Density Functional Theory Study of Reactions during HF Exposure. *Chem. Mater.* **2018**, *30*, 5912−5922.

(22) George, S. M.; Lee, Y. Prospects for Thermal Atomic Layer Etching Using Sequential, Self-Limiting Fluorination and Ligand-Exchange Reactions. *ACS Nano* **2016**, *10*, 4889−4894.

(23) Clancey, J. W.; Cavanagh, A. S.; Smith, J. E. T.; Sharma, S.; George, S. M. Volatile Etch Species Produced during Thermal Al_2O_3 Atomic Layer Etching. *J. Phys. Chem. C* **2020**, *124*, 287−299.

(24) Helms, C. R.; Deal, B. E. Mechanisms of the HF/H_2O Vapor-Phase Etching of SiO_2. *J. Vac. Sci. Technol., A* **1992**, *10*, 806−811.

(25) Williams, K. R.; Gupta, K.; Wasilik, M. Etch Rates for Micromachining Processing - Part II. *J. Microelectromech. Syst.* **2003**, *12*, 761−778.

(26) Williams, K. R.; Muller, R. S. Etch Rates for Micromachining Processing. *J. Microelectromech. Syst.* **1996**, *5*, 256−269.

(27) Winters, H. F.; Coburn, J. W. Etching of Silicon with XeF_2 Vapor. *Appl. Phys. Lett.* **1979**, *34*, 70−73.

(28) Lee, Y.; Huffman, C.; George, S. M. Selectivity in Thermal Atomic Layer Etching Using Sequential, Self Limiting Fluorination and Ligand-Exchange Reactions. *Chem. Mater.* **2016**, *28*, 7657−7665.

(29) Fischer, A.; Routzahn, A.; Lee, Y.; Lill, T.; George, S. M. Thermal Etching of AlF_3 and Thermal Atomic Layer Etching of Al_2O_3. *J. Vac. Sci. Technol., A* **2020**, *38*, 022603.

(30) Zhang, Z.; Pan, Y.; Yang, J.; Jiang, Z.; Fang, H. Experimental study of trimethyl aluminum decomposition. *J. Cryst. Growth* **2017**, *473*, 6−10.

(31) Chittock, N. J.; Vos, M. F. J.; Faraz, T.; Kessels, W. M. M.; Knoops, H. C. M.; Mackus, A. J. M. Isotropic Plasma Atomic Layer Etching of Al_2O_3 Using a Fluorine Containing Plasma and $Al(CH_3)_3$. *Appl. Phys. Lett.* **2020**, *117*, 162107.

(32) Gupta, P.; Coon, P. A.; Koehler, B. G.; George, S. M. Adsorption and Desorption Kinetics for $SiCl_4$ on $Si(111)7 \times 7$. *J. Chem. Phys.* **1990**, *93*, 2827−2835.

(33) Gupta, P.; Mak, C. H.; Coon, P. A.; George, S. M. Oxidation Kinetics of Si(111)7 × 7 in the Submonolayer Regime. *Phys. Rev. B: Condens. Matter Mater. Phys.* **1989**, *40*, 7739−7749.

(34) King, D. A.; Wells, M. G. Reaction Mechanism in Chemisorption Kinetics - Nitrogen on (100) Plane of Tungsten. *Proc. R. Soc. London, Ser. A* **1974**, *339*, 245−269.

(35) Palko, A. A.; Ryon, A. D.; Kuhn, D. W. The Vapor Pressures of Zirconium Tetrachloride and Hafnium Tetrachloride. *J. Phys. Chem.* **1958**, *62*, 319−322.

(36) Tangri, R. P.; Bose, D. K. Vapor Pressure Measurement of Zirconium Chloride and Hafnium Chloride by the Transpiration Technique. *Thermochim. Acta* **1994**, *244*, 249−256.

(37) Wu, M. M.; Wang, H.; Ko, Y. J.; Wang, Q.; Sun, Q.; Kiran, B.; Kandalam, A. K.; Bowen, K. H.; Jena, P. Manganese-Based Magnetic Superhalogens. *Angew. Chem., Int. Ed.* **2011**, *50*, 2568−2572.

(38) Karakaya, C.; Ricote, S.; Albin, D.; Sánchez-Cortezón, E.; Linares-Zea, B.; Kee, R. J. Thermogravimetric analysis of $InCl_3$ sublimation at atmospheric pressure. *Thermochim. Acta* **2015**, *622*, 55−63.

(39) Kabesh, A.; Nyholm, R. S. 716. Studies in co-ordination chemistry. Part X. The vapour pressure and heats of vaporisation of the stannic halides. *J. Chem. Soc.* **1951**, 3245−3252.

(40) Stull, D. R. Vapor Pressure of Pure Substrances. Inorganic Compounds. *Ind. Eng. Chem.* **1947**, *39*, 540−550.

(41) Bahlawane, N.; Reilmann, F.; Salameh, L.-C.; Kohse-Höinghaus, K. Mass-spectrometric monitoring of the thermally induced decomposition of trimethylgallium, tris(tert-butyl)gallium, and triethylantimony at low pressure conditions. *J. Am. Soc. Mass Spectrom.* **2008**, *19*, 947−954.